

The effect of coupling between CLUBB turbulence scheme and surface momentum flux on global wind simulations

Emanuele Silvio Gentile¹, Ming Zhao², Vincent E. Larson^{3,4}, Colin Zarzycki⁵, Zhihong Tan¹

¹Program in Atmospheric and Oceanic Sciences, Princeton University, 300 Forrester Road, Princeton, 08540, New Jersey, United States

²Geophysical Fluid Dynamics Lab, NOAA, 201 Forrester Road, Princeton, 08540, New Jersey, United States

³Department of Mathematical Sciences, University of Wisconsin–Milwaukee, Milwaukee, Wisconsin Pacific Northwest National Laboratory, Richland, Washington

⁴Pacific Northwest National Laboratory, Richland, Washington

⁵Department of Meteorology and Atmospheric Science, The Pennsylvania State University, University Park, Pennsylvania

Key Points:

- Dynamic coupling between CLUBB and surface momentum flux enhances global wind climate simulations bringing CLUBB in line with control AM4.
- In midlatitude regions, the dynamic coupling enhances the boundary-layer momentum transport compared to the static coupling.
- The wind turning angle turns out a useful qualitative metric, linking changes in surface momentum flux to the changes in global circulation.

Corresponding author: Emanuele Silvio Gentile, eg3736@princeton.edu

Abstract

The higher-order turbulence scheme, Cloud Layers Unified by Binormals (CLUBB), is known for effectively simulating the transition from cumulus to stratocumulus clouds within leading atmospheric climate models. This study investigates an underexplored aspect of CLUBB: its capacity to simulate near-surface winds and the Planetary Boundary Layer (PBL), with a particular focus on its coupling with surface momentum flux. Using the GFDL atmospheric climate model (AM4), we examine two distinct coupling strategies, distinguished by their handling of surface momentum flux during the CLUBB's stability-driven substepping performed at each atmospheric time step. The static coupling maintains a constant surface momentum flux, while the dynamic coupling adjusts the surface momentum flux at each CLUBB substep based on the CLUBB-computed zonal and meridional wind speed tendencies. Our 30-year present-day climate simulations (1980-2010) show that static coupling overestimates 10-m wind speeds compared to both control AM4 simulations and reanalysis, particularly over the Southern Ocean (SO) and other midlatitude ocean regions. Conversely, dynamic coupling corrects the static coupling 10-m winds biases in the midlatitude regions, resulting in CLUBB simulations achieving there an excellent agreement with AM4 simulations. Furthermore, analysis of PBL vertical profiles over the SO reveals that dynamic coupling reduces downward momentum transport, consistent with the found wind-speed reductions. Instead, near the tropics, dynamic coupling results in minimal changes in near-surface wind speeds and associated turbulent momentum transport structure. Notably, the wind turning angle serves as a valuable qualitative metric for assessing the impact of changes in surface momentum flux representation on global circulation patterns.

Plain Language Summary

The Cloud Layers Unified by Binormals (CLUBB) scheme offers a promising way to model the complexities of cloud behaviour, but its impact on winds and global circulation has been less explored. In our study, we investigate how different ways of representing the complex coupling between surface drag and the lowest kilometre of the Earth's atmosphere affect global wind speeds and circulation. We specifically examine two distinct approaches: a static approach, which feeds a constant surface drag to CLUBB, and a dynamic approach, which adjusts the surface drag based on the winds updates computed by CLUBB. Over a present-day climate, we find that static coupling tends to produce excessively large wind speeds in certain regions, like the Southern Ocean and parts of the North Atlantic and North Pacific. Instead, dynamic coupling produces excellent near-surface wind speeds in these regions, and also over the rest of the globe. Moreover, we discover that dynamic coupling reduces the downward turbulent transport of momentum, highlighting the enhancements in near-surface wind speeds found with this approach are physically consistent. Lastly, we use the change in wind direction with height to qualitatively evaluate how the two coupling methods affect global circulation patterns.

1 Introduction

General circulation models (GCMs) are pivotal in climate science but continue to present significant uncertainties when simulating clouds and turbulent transport within the Planetary Boundary Layer (PBL). These uncertainties hinder the representation of various fundamental atmospheric processes, affecting our understanding and ability to predict the Earth's climate, including the energy and hydrological cycles (Palmer, 2014; Slingo et al., 2022), PBL momentum transport, and surface wind speeds (Edwards et al., 2020).

Leading GCMs currently employ various regime-dependent schemes to represent deep convection, shallow convection, cloud processes, and PBL turbulence (Bush et al., 2020; Danabasoglu & et al., 2020; Zhao & et al, 2018). While these schemes have substantially advanced our comprehension (and modeling ability) of atmospheric dynamics, they exhibit limitations in representing atmospheric phenomena that inherently manifest as a gradual

rather than an abrupt transition between different regimes (Guo et al., 2015), such as from coastal stratocumuli to shallow cumuli clouds (Wyant et al., 1997). To address this gap, several regime-independent approaches have been introduced, such as super-parameterized GCMs (Khairoutdinov & Randall, 2001; Randall et al., 2003), Eddy Mass Flux Schemes, (Siebesma et al., 2007; Han et al., 2016; Tan et al., 2018) and km-scale global storm-resolving climate models (GSRMs) (Stevens et al., 2019; Slingo et al., 2022; Bolot et al., 2023). Despite their capacity to explicitly represent deep convection, the practical application of both super-parameterized GCMs and km-scale GSRMs remains often constrained by their significant computational demands (Harris et al., 2023), posing challenges for climate studies. Furthermore, km-scale GSRMs still rely on regime-dependent schemes to parameterize the PBL turbulent transport of heat, moisture, and momentum (Schär et al., 2020).

In light of these challenges, a new methodology has emerged (Randall et al., 1992; Lappen & Randall, 2001; Lappen et al., 2010) that aims to accurately model the subgrid variances of turbulent fluxes within clouds and the PBL, across diverse dynamic regimes, by using a joint probability density function (PDF) to prognose multiple higher-order moments encompassing subgrid variations in vertical velocity, temperature, and moisture. Among the higher-order parametrizations derived from this approach, three schemes stand out: CLUBB (Cloud Layers Unified By Binormals) (Golaz et al., 2002a, 2002b; Larson & Golaz, 2005; Larson et al., 2012, 2019), IPHOC (Intermediately Prognostic Higher-Order Closure) (Cheng & Xu, 2008), and Simplified Higher-Order Closure (Bogenschutz & Krueger, 2013). Despite a shared parametrization philosophy, both IPHOC and SHOC present limitations and drawbacks compared to CLUBB: IPHOC is characterized by its explicit numerics which necessitates a timestep tightly constrained to 30 s or less, posing computational speed challenges. On the other hand, SHOC, though faster than CLUBB, does not include certain terms crucial for adequately deepening shallow cumulus layers, thereby limiting its applicability in representing these specific cloud dynamics.

The higher-order CLUBB scheme, representing two decades of substantial development efforts, has been successfully integrated in two prominent GCM families: NCAR CAM5 (Bogenschutz et al., 2013; Wang et al., 2015) and GFDL AM3 (Guo et al., 2014, 2015). To align with the atmospheric timestep of these GCMs, CLUBB is substepped within the larger atmospheric timestep, ensuring detailed and accurate representation of sub-grid scale cloud processes. Specifically over the Eastern subtropical oceans where the low cloud regime transitions from stratocumulus to trade wind cumulus phenomena, CAM5-CLUBB has demonstrated a more gradual and realistic transition between these two cloud regimes, leading to a more close agreement with Clouds and the Earth’s Radiant Energy System (CERES) satellite observations (Bogenschutz et al., 2013). Similarly, AM3-CLUBB has shown enhanced capabilities, compared to AM3, in simulating the transition not only from stratocumulus to cumulus clouds, but also from shallow to deep cumulus clouds. However, despite the advances, challenges persist, particularly in accurately representing mixed-phase clouds and ice microphysics (Guo et al., 2015; Zhao & et al, 2018).

While the CLUBB model’s ability to represent cloud processes and feedbacks has been extensively documented in literature, its effectiveness in simulating near-surface wind speeds and associated PBL turbulent momentum transport has received less attention, with a few exceptions (Nardi et al., 2022). Particularly, the representation of surface drag within CLUBB and its consequent impact on near-surface wind speeds remain relatively unexplored. This knowledge gap persists despite numerous studies underscoring the importance of surface drag representation in PBL schemes for influencing midlatitude atmospheric dynamical processes; more specifically controlling the latitude of near-surface westerlies, the associated eddy-driven midlatitude jet (Gang et al., 2007), as well as the angle of wind turning and the cross-isobaric flow, which in turn impacts the formation and evolution of midlatitude cyclones (Svensson & Holtslag, 2009; Lindvall & Svensson, 2019). Indeed, the angle of wind turning has emerged as a useful metric to understand how changes in surface

drag and PBL turbulence representation in different CMIP6 models may contribute to the observed discrepancies in model global circulation outputs (Pyykkö & Svensson, 2023).

In this study, we investigate the impact of an accurate representation of surface momentum flux (or surface drag) on the simulation of near-surface winds and PBL structure when parametrizing PBL turbulence and clouds with the higher-order scheme CLUBB. Towards this aim we set up two distinct coupling strategies between surface momentum flux and the CLUBB higher-order closure scheme when integrated within the leading GFDL climate model AM4 (Zhao & et al, 2018). These strategies are differentiated by their approach of handling surface momentum flux during CLUBB’s stability driven substepping performed at each atmospheric timestep. The first strategy, implemented in the AM4-CLUBB.1 configuration, hereafter referred to as “static coupling”, maintains a constant surface momentum flux throughout CLUBB’s sub-stepping. In contrast, the second strategy, implemented in the AM4-CLUBB.2 configuration, hereafter referred as “dynamic coupling”, updates the surface momentum flux at each CLUBB substep, aligning it with the corresponding CLUBB-computed zonal and meridional wind speed tendencies. We hypothesize that dynamic coupling can more accurately capture the nonlinear interactions between the surface momentum flux, near-surface winds, and the associated PBL structure, since it allows CLUBB-simulated sub-grid turbulence to dynamically respond to changes in surface drag. To test our hypothesis, we conduct a present-day 30-year climate integration from 1980 to 2010 using both AM4-CLUBB.1 and AM4-CLUBB.2 configurations, and we systematically compare and analyze the near-surface wind speeds and PBL structure simulated by these two model configurations against the operational configuration of AM4 (Zhao & et al, 2018). Moreover, we qualitatively evaluate how changes in the representation of surface momentum flux (or surface drag) between AM4-CLUBB.1 and AM4-CLUBB.2 impact the global circulation using the wind turning angle metric.

The remainder of this article is organised as follows. Section 2 discusses the GFDL Atmospheric Climate Model AM4, detailing the two different coupling strategies, static and dynamic, between surface momentum flux and CLUBB, and introduces the physical formulation of the wind turning angle. Section 3 analyzes the impact of the two coupling strategies on near-surface wind speeds and associated PBL structure is analyzed, along with its broader implications for the global circulation. Finally, conclusions are drawn Section 4.

2 Methods

2.1 Overview of the GFDL AM4 model

Our investigation of CLUBB ability to simulate near-surface wind speeds employs as a framework the GFDL AM4 model, the most advanced iteration of the GFDL series of atmospheric climate models (Zhao & et al, 2018). The model features a cubed-sphere topology within its atmospheric dynamical core, with a refined horizontal grid consisting of 96×96 grid cells per cube face, resulting in an approximate resolution of ≈ 100 km. This refinement marks a significant enhancement over its predecessors, AM2 and AM3, which utilized a coarser ≈ 200 km horizontal grid spacing.

Structured with 33 vertical levels and reaching up to 1 hPa, the GFDL AM4 model includes a sponge layer extending down to 8 hPa. The vertical stratification mirrors that of AM3 in the troposphere but incorporates an additional layer near the surface to more accurately represent the Earth’s surface. The model employs the hydrostatic version of the FV3 finite-volume cubed-sphere dynamical core, with minor modifications from the version used in AM3. The AM4 model parameterizations of the PBL surface and cloud macrophysics are akin to AM3. The model parametrizes PBL turbulence using a first-order eddy diffusion closure Lock scheme (Lock et al., 2000), while cloud macrophysics follows a prognostic scheme for stratiform and convective clouds (Tiedtke, 1993), where cloud dynamics are governed by large-scale budget equations for cloud water content and cloud air. Within

the surface layer, AM4 employs Monin-Obukhov bulk transfer formulations and executes central differencing in the outer layer, determining diffusion coefficients based on flux levels between model levels (Lock et al., 2000). The interaction between the atmosphere and land is modeled through an implicit coupling, akin to AM3. More specifically, the PBL scheme implicitly updates the zonal and meridional turbulent surface momentum fluxes and winds at each atmospheric timestep, resolving a tridiagonal matrix system that arises from the numerical discretization of the advection-diffusion equation for momentum (and similarly for heat and moisture). This system encompasses both atmospheric levels and the top layer of the land surface scheme, including the tiles (Polcher & et al, 1998; Best et al., 2004).

Furthermore, the GFDL AM4 model incorporates significant advancements in radiation treatment, moist convection, orographic gravity wave drag, aerosol module structure, and cloud microphysics (Zhao & et al, 2018). Notably, the GFDL AM4 model has participated in the CMIP6 High-Resolution Model Intercomparison Project (Haarsma & et al, 2016; Zhao & et al, 2018), highlighting its prominence and suitability for state-of-the-art climate research.

2.2 Brief description of CLUBB and its integration in the GFDL AM4 model

CLUBB is a higher-order parametrization scheme, unifying the modeling of cloud dynamics and PBL turbulence. It directly prognoses mean vertical upward wind speed \bar{w} , total water mixing ratio \bar{r}_t , mean liquid water potential temperature $\bar{\theta}_l$, turbulent heat and moisture fluxes $\overline{w'\theta'_l}$ and $\overline{w'r'_l}$, covariance of first order moments of total water mixing ratio and potential temperature $\overline{r'_l\theta'_l}$, liquid water potential temperature and total water mixing ratio variances $\overline{\theta'^2_l}$ and $\overline{r'^2_t}$, vertical upwind variance $\overline{w'^2}$, and third-order moment of upward wind $\overline{w'^3}$. A key aspect of CLUBB's approach is the employment of a joint probability density function (PDF) of vertical velocity, temperature, and moisture, selected from a family of PDFs to achieve closure of higher-order turbulent moments and buoyancy terms. The preferred PDF assumes the form of a double normal-lognormal Gaussian distribution (Golaz et al., 2002a, 2002b).

In this study, CLUBB has been integrated into AM4, with the CLUBB parametrization invoked within the sequence of moist processes parameterizations. Specifically, it operates after the deep convection scheme (Donner et al., 2001) and before the microphysics scheme (Rotstayn, 1997), in place of the cloud macrophysics scheme, aligning with the previous implementation of CLUBB in the GFDL AM3 model as CLUBB-AM3 (Guo et al., 2015). A critical aspect of CLUBB integration involves the management of different timesteps. As detailed in the context of AM3-CLUBB (Guo et al., 2015), CLUBB's timestep is set to $\Delta t_{CLUBB} = 120$ s, due to stability requirements. This is significantly shorter than AM4's atmospheric timestep, $\Delta t_{atmos} = 1800$ s. Thus, CLUBB operates with substepping within the atmospheric loop of AM4.

In our integration of CLUBB into AM4, turbulent heat and moisture fluxes are directly prognosed by CLUBB, while the vertical zonal and meridional momentum fluxes, $\overline{u'w'}$ and $\overline{v'w'}$ respectively, are diagnosed in this version of CLUBB integrated in AM4, assuming a simple downgradient flux closure as follows:

$$\begin{aligned}\overline{u'w'} &= -K_m \frac{\partial \bar{u}}{\partial z} \\ \overline{v'w'} &= -K_m \frac{\partial \bar{v}}{\partial z}\end{aligned}\tag{1}$$

Here, u and v represent the grid-box mean zonal and meridional wind speeds, respectively, z is the vertical coordinate and K_m denotes the eddy diffusivity coefficient. Specifically, CLUBB calculates K_m based as:

$$K_m = c_k L \bar{e}^{1/2}\tag{2}$$

where $\bar{\epsilon}$ represents the turbulent kinetic energy, c_k is a constant (set to 0.5 here), and L denotes the turbulent length scale, a key factor in CLUBB indicating the extent to which a parcel can move vertically due to buoyancy effects (Golaz et al., 2002a, 2002b). It is crucial to note that the K_m computed by CLUBB with Eq. 2 is distinct from the K_m computed in the AM4 PBL parametrization by the Lock scheme (Lock et al., 2000). Given the discrepancy between CLUBB and Lock K_m formulations, to diagnose and quantify the vertical mixing of momentum we use the following effective eddy diffusivity formulation (Bryan et al., 2017):

$$K_m = \frac{\sqrt{(\overline{u'w'})^2 + (\overline{v'w'})^2}}{\sqrt{(\frac{\partial u}{\partial z})^2 + (\frac{\partial v}{\partial z})^2}} \quad (3)$$

2.3 Coupling strategies between CLUBB and surface momentum flux

The inherent architecture of CLUBB necessitates explicit coupling between the surface (over land/ice/ocean) momentum flux and the PBL. The most straightforward approach, offering computational efficiency when CLUBB is integrated into the AM4 framework, provides surface fluxes directly to CLUBB and keeps these values constant throughout CLUBB's substepping performed at each atmospheric timestep. This approach has been widely adopted in configurations like CAM5-CLUBB and AM3-CLUBB (Guo et al., 2015; Bogenschutz et al., 2013). However, we hypothesize, in this study, that dynamically updating the surface momentum flux (surface drag) at each CLUBB substep, could more accurately capture the intricate non-linear interactions between the surface momentum flux, near-surface winds, and the PBL structure.

To effectively integrate CLUBB into AM4 and assess the impact of different coupling strategies between CLUBB and surface momentum flux on the performance of AM4 in simulating near-surface winds and the PBL, we established two distinct configurations of AM4-CLUBB, named AM4-CLUBB_1 and AM4-CLUBB_2, each implementing a unique coupling strategy between CLUBB and surface momentum flux. The first configuration, AM4-CLUBB_1, embodies a static coupling approach, similar to AM3-CLUBB, that maintains a consistent surface momentum flux throughout CLUBB's substepping at each atmospheric timestep $\Delta t_{atmos} = 1800$ s, as visualized in Fig 2a. In contrast, the second configuration, AM4-CLUBB_2, employs a dynamic coupling approach that recalculates the surface momentum flux at each CLUBB substep $\Delta t_{CLUBB} = 120$ s based on the evolving CLUBB-computed zonal and meridional wind speed tendencies, as illustrated in Fig 2b. More specifically, the surface momentum flux is dynamically updated at each CLUBB substep Δt_{CLUBB} according to the following equations:

$$\begin{aligned} \overline{u'w'} &= \tau_x / \rho = -C_d u_1 |\mathbf{V}_1| \\ \overline{v'w'} &= \tau_y / \rho = -C_d v_1 |\mathbf{V}_1| \end{aligned} \quad (4)$$

where τ_x and τ_y denote the zonal and meridional surface stresses, C_d is the drag coefficient, ρ is the surface air density, and u_1 and v_1 represent the lowest-model atmospheric level wind speeds. These wind speeds are recalculated at each substep $\Delta t_{CLUBB} = 120$ s, based on the updated CLUBB tendencies, with $|\mathbf{V}_1| = \sqrt{u_1^2 + v_1^2}$ indicating the magnitude of the total wind vector at the lowest atmospheric level, while C_d is held constant within CLUBB substepping to maintain consistency with other model components.

2.4 Summary of experimental set up

To assess the impact of the coupling between surface momentum flux and CLUBB on the global simulation of near-surface winds and PBL momentum transport, we utilized the GFDL-AM4 configuration as a baseline, referred to AM4 for sake of simplicity, which aligns with the model specifications detailed in Sect 2.1. In addition, we used the two model configurations (with CLUBB integrated in AM4) based on the coupling strategies

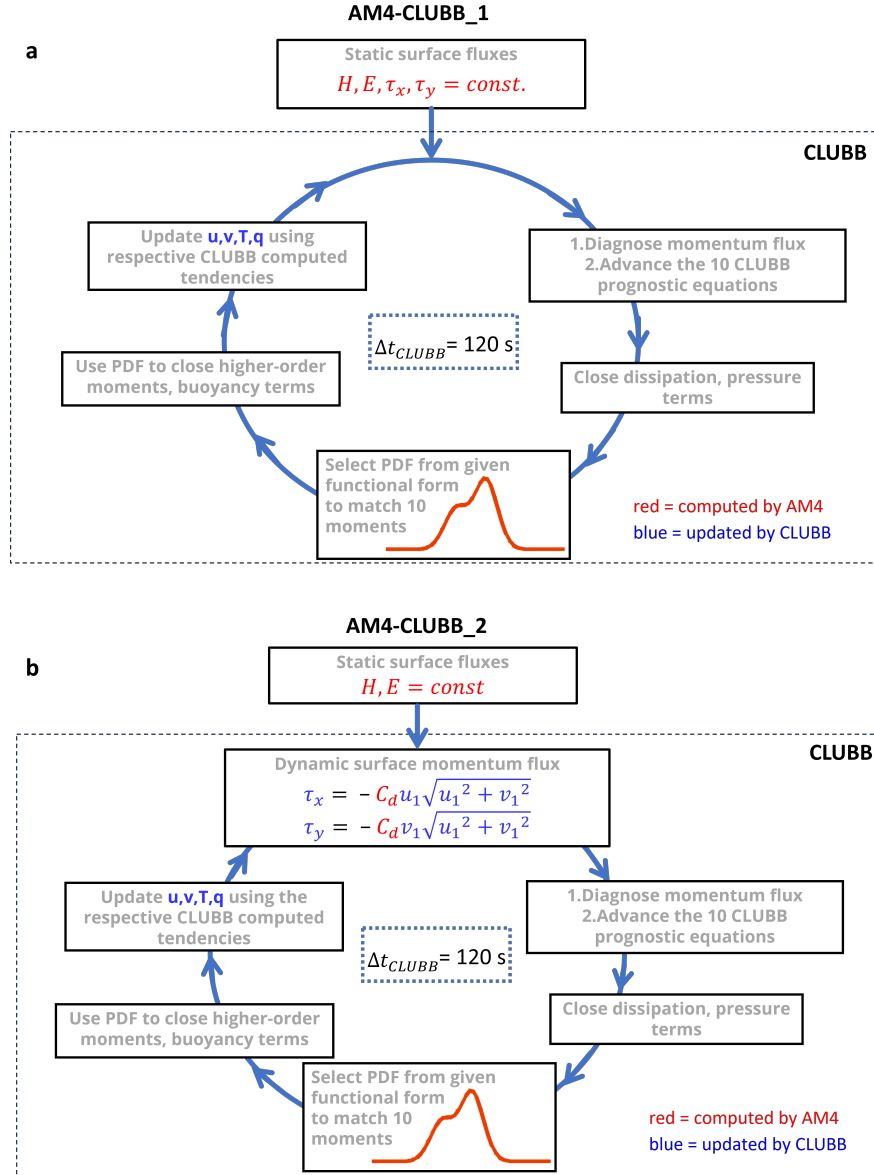


Figure 1. Illustration of coupling strategies in AM4-CLUBB. (a) Static coupling (AM4-CLUBB.1): the surface momentum flux is maintained constant throughout CLUBB’s sub-stepping covering the atmospheric timestep $\Delta t_{\text{atmos}} = 1800 \text{ s}$. (b) Dynamic coupling (AM4-CLUBB.2): the surface momentum flux is dynamically updated at each CLUBB substep, $\Delta t_{\text{CLUBB}} = 120 \text{ s}$, using the CLUBB-computed wind speed tendencies.

described in Sect 2.2: AM4-CLUBB.1, which employs the static surface momentum flux coupling strategy, and AM4-CLUBB.2, which incorporates the dynamic coupling strategy as per Eq. 4. For this study, the three configurations—AM4, AM4-CLUBB.1, and AM4-CLUBB.2— were utilized and compared across climatological runs spanning the present-day 30-year period 1980-2010. Throughout this period, radiative forcing agents were held constant at 2010 levels, while sea surface temperatures (SSTs) and sea-ice concentrations were averaged based on the data from 1981 to 2014, adhering to CMIP6 protocols (Haarsma & et al, 2016). Notably, the AM4 model’s simulation of present day climatology, using these specified SSTs, sea-ice concentrations, and fixed radiative forcings, demonstrates close alignment with the corresponding AMIP simulation outcomes (Zhao & et al, 2018). This alignment makes the three configurations —AM4, AM4-CLUBB 1, and AM4-CLUBB 2— particularly apt for a qualitative assessment of how the dynamic coupling between CLUBB and the surface momentum flux impact on model’s accuracy in simulating 10-meter wind speed when compared against reanalysis data. Specifically, for the evaluation of 10-m wind speed skill of the AM4 configurations, our study references the European Centre for Medium-range Weather Forecasts (ECMWF) fifth generation hourly reanalysis, ERA5 (Hersbach et al., 2020), as the standard for comparison. This approach allows a comprehensive analysis of the effectiveness and implications of different CLUBB coupling strategies on the fidelity of 10-m wind speed predictions in the AM4 model.

2.5 Wind turning angle metric

Recent literature has recognized the angle of wind turning as an important metric for linking changes in surface drag and their subsequent effects on PBL stratification, and by extension, to PBL height, latitudinal variations, the Rossby number, and even the magnitude of wind speed itself (Lindvall & Svensson, 2019; Pyykkö & Svensson, 2023). In this section, we discuss further the wind turning angle metric.

The angle of wind turning is quantified as the shift in wind direction from the surface level to the first level just above the PBL top. This angle is considered positive for a clockwise turn with increasing altitude. To ensure uniformity in representation, wind turning angles are standardized to lie within the -180° to 180° range, adjusting through the addition or subtraction of 360° as needed.

From a theoretical standpoint, the wind turning angle aligns closely with the surface cross-isobaric angle. This assumption holds particularly when the wind near the PBL top approximates geostrophic behavior and exhibits negligible directional change with altitude. Consequently, the wind’s vertical veering within the PBL emerges as an useful metric for investigating how changes in surface drag representation across various model configurations influence cross-isobaric flow. These changes bear implications for the formation of cyclones and the dynamics of large-scale atmospheric circulation.

An analytical expression for the angle of wind turning, denoted as α , can be derived under certain assumptions (Svensson & Holtslag, 2009). These assumptions include distinguishing between the mean and turbulent components of the flow, negligible divergence of horizontal turbulent flux, omission of molecular viscosity, and the momentum flux being negligible at the top of the PBL, denoted as ‘h’. Following these approximations, an analytical expression for α is developed, linking the angle of wind turning with key atmospheric variables. This expression correlates the cross-isobaric flow, represented by the averaged ageostrophic wind $\langle \bar{v} \rangle$, with the boundary layer height ‘h’, the surface momentum flux u_*^2 (where $u_*^2 = \sqrt{(-u'w'_0)^2 + (-v'w'_0)^2}$), and the wind turning angle α , as described by the equation:

$$fh \langle \bar{v} \rangle = u_*^2 \cos(\alpha) \quad (5)$$

where f represents the Coriolis parameter. The significance of Eq. 5 lies in its ability to relate the cross-isobaric mass flux to the angle of wind turning, given known values of turbulent surface momentum flux and PBL height. This allows for a deeper understanding of how the

representation of surface drag, particularly the turbulent surface momentum flux, influences large-scale atmospheric circulation patterns.

3 The impact of coupling CLUBB with surface momentum flux on global winds, surface stress, and boundary-layer height in AM4

In this analysis, we start by directly comparing the 10-m wind speeds predicted by the AM4 model against the reference ERA5 reanalysis data (Hersbach et al., 2020). This establishes a baseline for performance assessment. Next, we perform a comparison between the AM4’s model configurations AM4-CLUBB.1, featuring static coupling, and AM4-CLUBB.2, featuring dynamic coupling, against the baseline control AM4 configuration. Although these two CLUBB-based configurations are not directly compared with the ERA5 data, their indirect comparison through AM4 allows us to assess their relative behavior against an accurate reanalysis benchmark.

The control AM4 model configuration’s annual mean 10-m wind speed for the 1980-2010 period visualized in Fig. 2a shows an overall good agreement with ERA5’s corresponding 10-m wind speeds illustrated in Fig. 2b. Over the oceans, the AM4 model’s bias remains confined within $\pm 2 \text{ m s}^{-1}$ compared to ERA5 data, underestimating 10-m wind speeds in the North Atlantic and North Pacific Ocean, while overestimating them in the Southern Ocean and the tropics. Over land, the bias narrows to within $\pm 0.5 \text{ m s}^{-1}$, except in regions characterized by high orography, such as Greenland, the Rocky Mountains, the Himalayan Mountains, and the coasts of Antarctica. Although ERA5 does not assimilate 10-m hourly winds over land (Molina et al., 2021), a plausible explanation for the underestimation of AM4 extreme wind speeds - compared to ERA5 data - over these mountains terrains lies in the AM4 model’s coarser resolution ($\approx 100 \text{ km}$) compared to the ERA5 finer resolution ($\approx 30 \text{ km}$), combined with an excessive orographic gravity wave drag within AM4 model.

Figure 2c-d illustrate that static coupling strategy between surface momentum flux and CLUBB (AM4-CLUBB.1) tends to generate more intense 10-m wind speeds than AM4 model, a discrepancy that is particularly marked in the midlatitudes over the oceanic regions. The Southern Ocean stands out as the region most significantly impacted by this overestimation, with AM4-CLUBB.1 simulating 10-m wind speeds exceeding 4 m s^{-1} , followed by the North Pacific and North Atlantic Oceans, where the overestimation reaches up to 2 m s^{-1} . In the tropics, the AM4-CLUBB.1 overestimation does not exceed 1 m s^{-1} , with the exception of the Southern Indian Ocean and the stretch of the Atlantic Ocean from Mexico to West Africa, (near 30°N), where AM4-CLUBB.1 forecasts 10-m wind speeds 1 to 2 m s^{-1} higher than AM4. Interestingly, in very few high-orography places, such as the coastlines of Greenland and Antarctica, the AM4-CLUBB.1 model’s simulated increases in 10-m wind speeds compensate for AM4’s underestimations in these regions when compared to ERA5, as can be inferred from Fig. 2b-d.

When employing the dynamic coupling strategy between surface momentum flux and CLUBB (AM4-CLUBB.2), a marked reduction in the 10-m wind speed bias relative to AM4 is observed, as demonstrated by the comparison of Fig. 2e and Fig. 2f. Moreover, a meticulous examination reveals that the AM4-CLUBB.2 configuration not only mitigates the biases relative to ERA5 noted in AM4-CLUBB.1, but also enhances the simulated 10-m wind speeds in comparison to the control AM4 simulation across several key geographical regions. For instance, in the Southern Ocean where AM4 overestimates 10-m wind speeds by up to 1 m s^{-1} compared to ERA5, AM4-CLUBB.2 decreases AM4 winds by up to 1 m s^{-1} , effectively reducing the control AM4 bias (with respect to ERA5). However, in a few localized regions, such as near 30°N (tropics) in the Atlantic Ocean and certain areas in the Indian Ocean and the Pacific Oceans where AM4 already exhibits a positive bias, AM4-CLUBB.2 further amplifies AM4 winds by up to 1 m s^{-1} , consequently further diminishing the accuracy of the original AM4 control simulation skill in these specific locations.

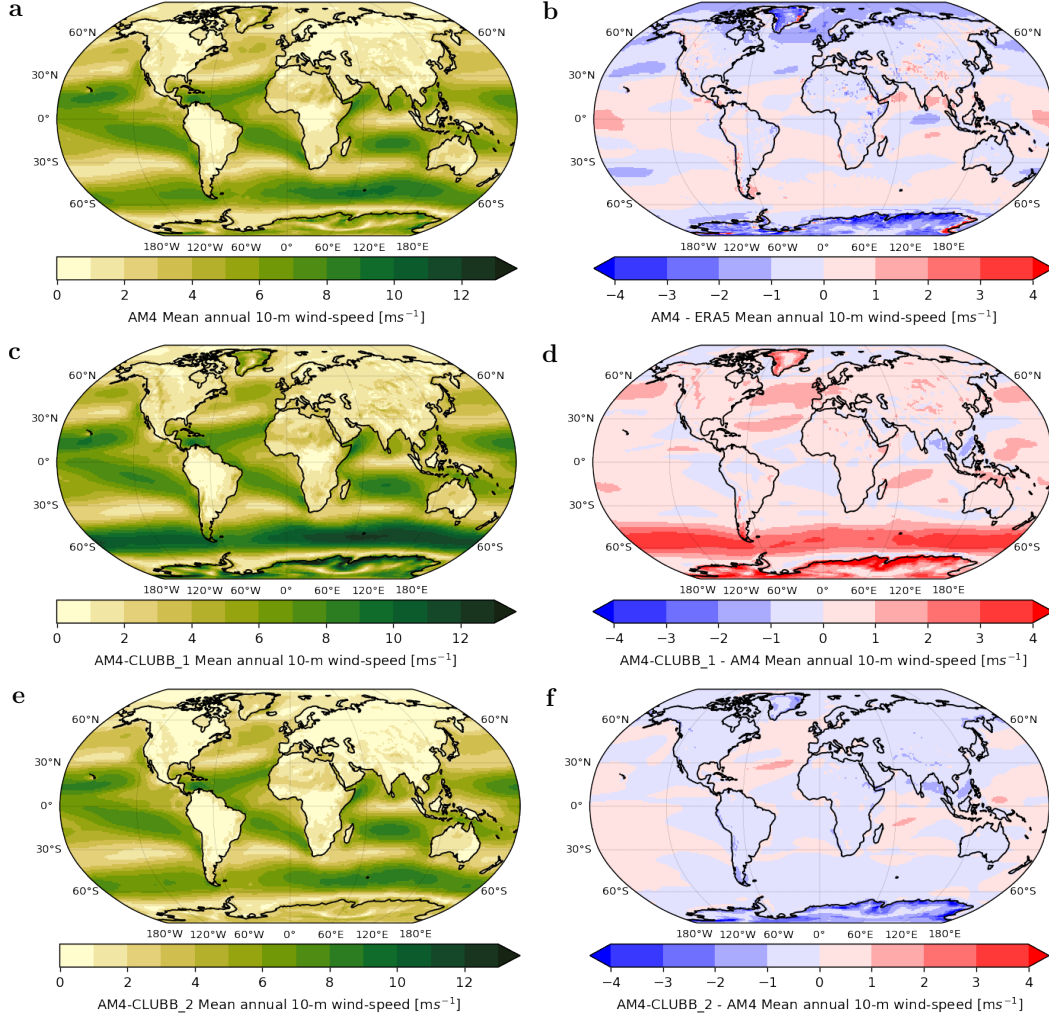


Figure 2. Comparative visualization of AM4, AM4-CLUBB.1, and AM4-CLUBB.2 10-m wind speeds. The left column illustrates the spatial distribution of annual mean 10-m wind speeds simulated by the (a) AM4 (c) AM4-CLUBB.1 (e) AM4-CLUBB.2 model configurations. The right column illustrates the spatial distribution of the annual mean 10-m wind speed difference between (b) AM4 (d) AM4-CLUBB.1 (f) AM4-CLUBB.2 and ERA5 corresponding values for the period 1980-2010.

To better understand the impact of static and dynamic coupling strategies on 10-m wind speed simulations, we examine the PBL surface characteristics associated with the annual mean 10-m wind speeds as simulated by AM4-CLUBB.1 and AM4-CLUBB.2. Analysis of the spatial distribution of surface stress as simulated by AM4-CLUBB.1, and its bias relative to AM4, as shown in Fig. 3a-b, reveals a positive correlation in areas where AM4-CLUBB.1 tends to overestimate surface wind speeds, particularly in the Southern Ocean and the North Atlantic. However, this pattern is not always homogeneous, for instance, between the Southern Ocean latitudes 30° and 50°S, the surface stress, τ , is reduced rather than increased. According to studies conducted with idealised dry GCM (Gang et al., 2007; Mbengue & Woollings, 2019), this reduction in effective surface drag coefficient (as indicated by the stronger increase in 10-m wind speed compared to τ), can lead to a circulation response of more poleward and stronger westerly jet, which aligns with the findings reported here. Moreover, over high-orography areas, such as the coasts of Antarctica and the Rocky

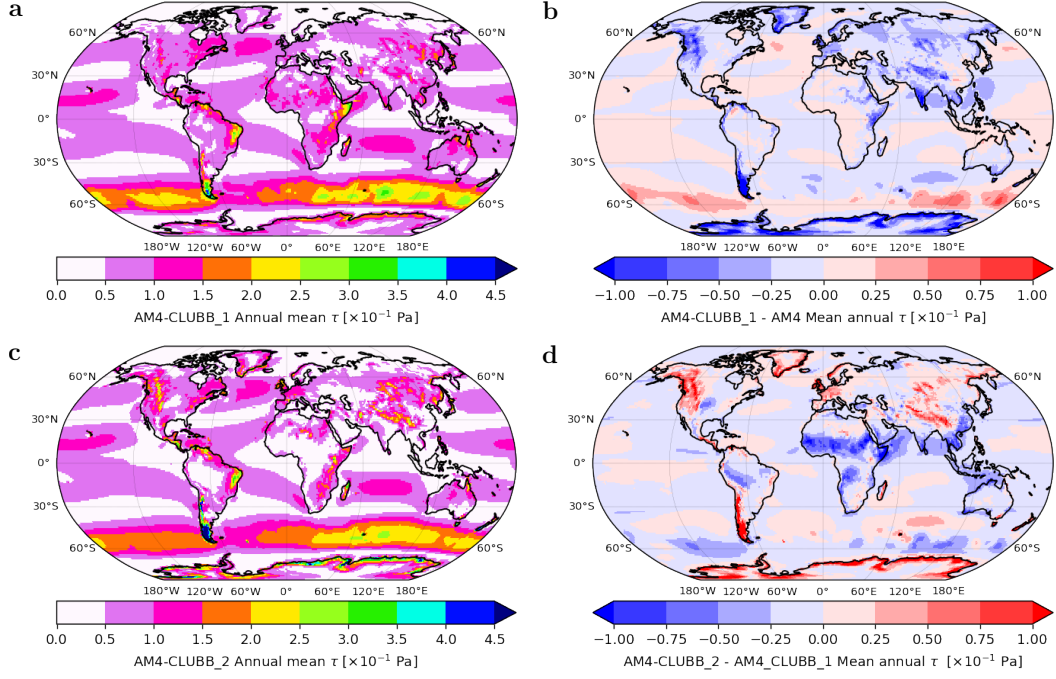


Figure 3. Spatial Analysis of Surface Stress. On the left column, spatial distribution of annual mean surface stress, τ , over the 1980-2010 period as simulated by (a) AM4-CLUBB_1 and (c) AM4-CLUBB_2. On the right column, the differences in τ , showing the deviation of (b) AM4-CLUBB_1 from the baseline AM4 model and (d) the changes when transitioning from AM4-CLUBB_1 to AM4-CLUBB_2.

Mountains, where AM4-CLUBB_1 overestimates surface wind speeds compared to AM4 (although not when compared to ERA5), the surface stress associated with these overestimations is lower than that observed in the AM4 model. However, when we transition to the dynamic coupling approach in AM4-CLUBB_2, as depicted in Fig. 3c-d, the bias in surface stress seen with AM4-CLUBB_1 is reversed across most regions, along with the poleward shift in surface stress, with the notable exception of equatorial Africa.

Mirroring the differences observed in surface stress between static coupling AM4-CLUBB_1 and control AM4, AM4-CLUBB_1 exhibits an increased PBL height h compared to AM4, particularly over the Southern Ocean and the tropics, as illustrated in Fig. 4. In contrast, regions such as Equatorial Africa, northern Australia, the Himalayas, and, to a lesser extent, the Rockies, experience shallower PBL height, h . As illustrated in Fig. 4a-b, the PBL height in AM4-CLUBB_1 can exhibit an overestimation of up to 300 m in the Southern Ocean when compared to AM4, while conversely experiencing an underestimation of a similar magnitude over the Himalayan mountain chain. However, the dynamic coupling, in AM4-CLUBB_2, between CLUBB and surface momentum flux demonstrates a marked improvement in these biases (these biases are effectively reversed, see Fig. 4c-d). In fact, dynamic coupling simulates a PBL shallower by 250 m than AM4-CLUBB_1 over the Southern Ocean, though changes in the PBL height on adopting a dynamic coupling strategy are negligible over the tropics, suggesting different atmospheric sensitivity.

Overall, the findings illustrated in Fig. 2, 3, and 4 demonstrate how the coupling of surface momentum flux, whether static and dynamic, influences the simulation of wind, stress, and PBL height, h , across various regions. In subtropical oceanic regions, the simulations show no significant variations in wind, stress, and PBL height due to changes in

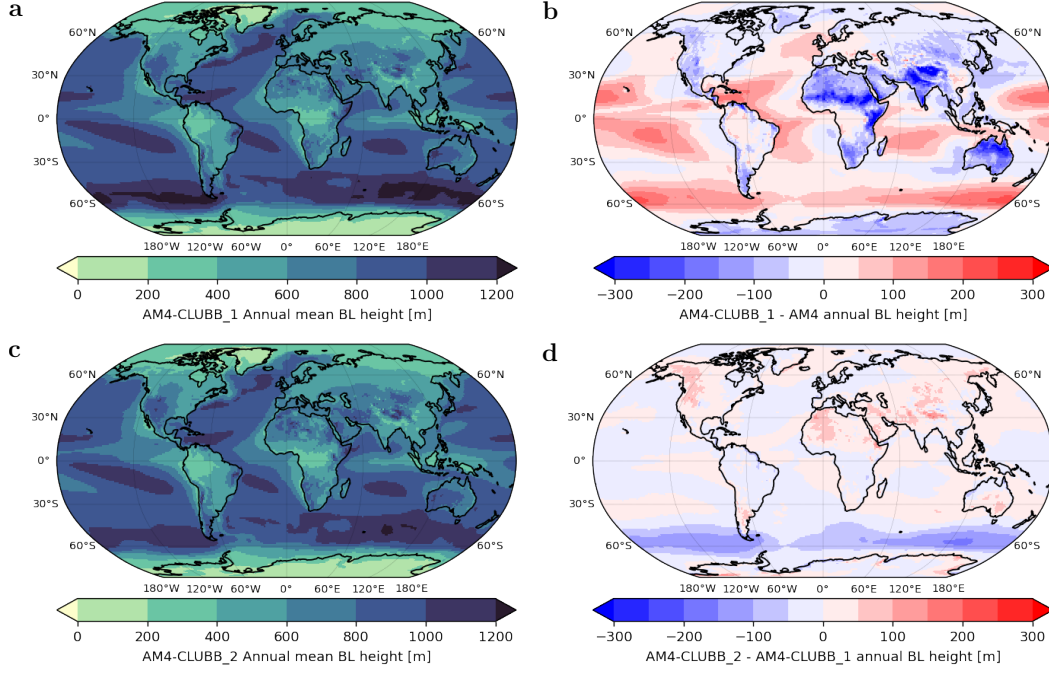


Figure 4. Comparative Analysis of Simulated PBL Heights. The left column presents the spatial distribution of PBL height as simulated by (a) AM4-CLUBB_1 and (c) AM4-CLUBB_2. The right column presents the spatial difference in PBL height between (b) AM4-CLUBB 1 and AM4 (d) AM4-CLUBB 2 and AM4-CLUBB 1. The PBL height is diagnosed using a “dynamic criterion” (Troen & Mahrt, 1986), whereby the boundary layer corresponds to the model-level height at which the Richardson number Ri exceeds the critical threshold of 0.25.

coupling strategy. However, a marked contrast is observed in midlatitude oceans, such as the Southern Ocean and the North Atlantic, where these atmospheric fields are significantly more responsive to the type of CLUBB-surface momentum flux coupling employed. In these regions, static coupling AM4-CLUBB_1 exhibits significantly increased 10-m wind speeds, surface stress, and PBL height when compared to both the original AM4 model configuration and AM4-CLUBB_2. Hence, it is plausible to hypothesize that the PBL in static coupling AM4-CLUBB_1 is more turbulent on an annual average basis than its counterparts AM4 and dynamic coupling AM4-CLUBB_2, as suggested by the heightened surface stress and PBL heights. Given that the Southern Ocean and the North Atlantic overlap with the major midlatitude storm tracks (Catto & et al, 2019), these two regions may experience intensified turbulence within the PBL in static coupling simulations. This heightened turbulence could correspond to a stronger eddy-diffusivity, potentially leading to a more efficient downward transport of momentum to the surface from the prevalent fast-flowing low-level jets (commonly associated with midlatitude cyclones in these regions) lying at the top of the PBL. Although downward transport of momentum may be stronger in AM4-CLUBB_1 than AM4-CLUBB_2, its divergence, corresponding to the zonal wind speed tendency due to PBL turbulent diffusion, may also be stronger, resulting in a more efficient damping of the zonal wind. Finally, large-scale dynamics forcing, besides downward momentum transport into the PBL and surface momentum flux (or drag) also affects the near-surface wind speed. Therefore, a thorough investigation of the vertical structure of the simulated PBL at specific locations as well as a cross-section analysis of the zonal winds over the Southern Ocean is essential to gain further insights on the differences between static coupling AM4-CLUBB_1 and dynamic coupling AM4-CLUBB_2 near surface wind speeds.

4 The impact of coupling CLUBB with surface momentum flux on boundary-layer momentum diffusion and wind vertical structure

To gain a deeper insight into the impact of the coupling strategies between surface momentum flux and CLUBB on near-surface wind speeds, we conduct a detailed analysis focusing on changes in the vertical diffusion profiles within the PBL at two points chosen for their representativeness of distinct responses of the coupling strategy: one point in the Southern Ocean, where the near-surface wind speeds exhibit a strong response to the choice of coupling strategy, and the other one in the tropics, where the near-surface wind speeds response to the coupling strategy is substantially smaller (as explored in detail in Sect. 3.1).

Figure 5 visualizes the zonal wind speed tendencies $\frac{\partial u}{\partial t}$ attributed to a spectrum of contributions: turbulent diffusion (labelled as “diff”), dynamics (labelled as “dyn”), and topography (labelled as “topo”), along with the effective eddy diffusivity coefficients, K_m , at the two representative locations in the Southern Ocean (Fig. 5a,c) and the tropics (Fig. 5b,d), respectively. Our findings in Fig. 5a,b indicate that in both selected locations, the tendencies $\frac{\partial u}{\partial t}$ due to turbulent diffusion (“diff”) across AM4, AM4-CLUBB.1, and AM4-CLUBB.2 have a negative sign and thus are opposite to the wind direction. Conversely, the tendencies $\frac{\partial u}{\partial t}$ due to the atmospheric dynamics, which include factors like the Coriolis effect and pressure gradients, have a positive sign, and thus act in the same direction as that of the wind. This implies that for the point in the Southern Ocean (dominated by westerlies) the turbulent diffusion tendencies lead to a negative (downward) zonal momentum flux, decelerating the winds, while for the point in the tropics (dominated by easterlies) the turbulent diffusion tendencies lead to a positive (upward) zonal momentum flux. Since the zonal wind speed tendencies oppose the turbulent diffusion tendencies, they act to accelerate the zonal flow in the selected Southern Ocean region and decelerate the flow in the selected tropics region. It is important to note that being both points over the sea, the topographic tendencies of all model configurations are zero, but we have included them for consistency in Fig. 5a-b.

In the Southern Ocean, static coupling AM4-CLUBB.1 demonstrates a marked increase in the turbulent diffusion tendencies compared to the control AM4 model, with a large maximum difference observed, reaching up to $-15 \times 10^{-5} \text{ m s}^{-2}$ (as depicted in Fig. 5a). Instead, dynamic coupling AM4-CLUBB.2 and AM4 present a roughly similar peak at $-10 \times 10^{-5} \text{ m s}^{-2}$, $\approx 33\%$ smaller than static coupling AM4-CLUBB.1. Comparing these tendencies with the effective eddy diffusivity coefficient, K_m , offers valuable insights into the effects of different coupling strategies on the atmospheric dynamics at play, particularly concerning turbulent momentum transport within the PBL. Figure 5c sheds light on the behaviour of K_m across the models. Within the PBL, static coupling AM4-CLUBB.1’s K_m significantly exceeds that of both AM4 and AM4-CLUBB.2, mirroring the observed tendencies in the wind speed profiles. More in details, AM4-CLUBB.2 K_m peaks at $15 \text{ m}^2 \text{ s}^{-1}$, in agreement with the corresponding AM4 peak k_m value, while AM4-CLUBB.1 peaks at $19 \text{ m}^2 \text{ s}^{-1}$, which is $\approx 25\%$ larger than the AM4 baseline. The fact that AM4-CLUBB.1 exhibits larger diffusive tendencies and increased effective eddy momentum diffusivity for the selected Southern Ocean point is consistent with the larger surface momentum flux previously found around 60°S latitude over the Southern Ocean (see Fig. 3). Indeed, the vertical integral of diffusive momentum tendency should equal the surface momentum flux. However, there are also locations in the Southern Ocean where the surface wind is slightly stronger in AM4-CLUBB.1 compared to AM4-CLUBB.2 but the surface stress is weaker, such as the point at 45°S , 60°E . At such locations the diffusion tendencies are weaker in AM4-CLUBB.1 compared to AM4-CLUBB.2 (not shown).

To further understand the influence of coupling strategy on the turbulent momentum transport and associated PBL stability and structure, we also investigate the wind and potential temperature profiles at the selected Southern Ocean point. The analysis of the vertical profiles of potential temperature shown in Fig. 6c for the point in the Southern Ocean highlights that, static stability in the PBL remains largely unaffected by chang-

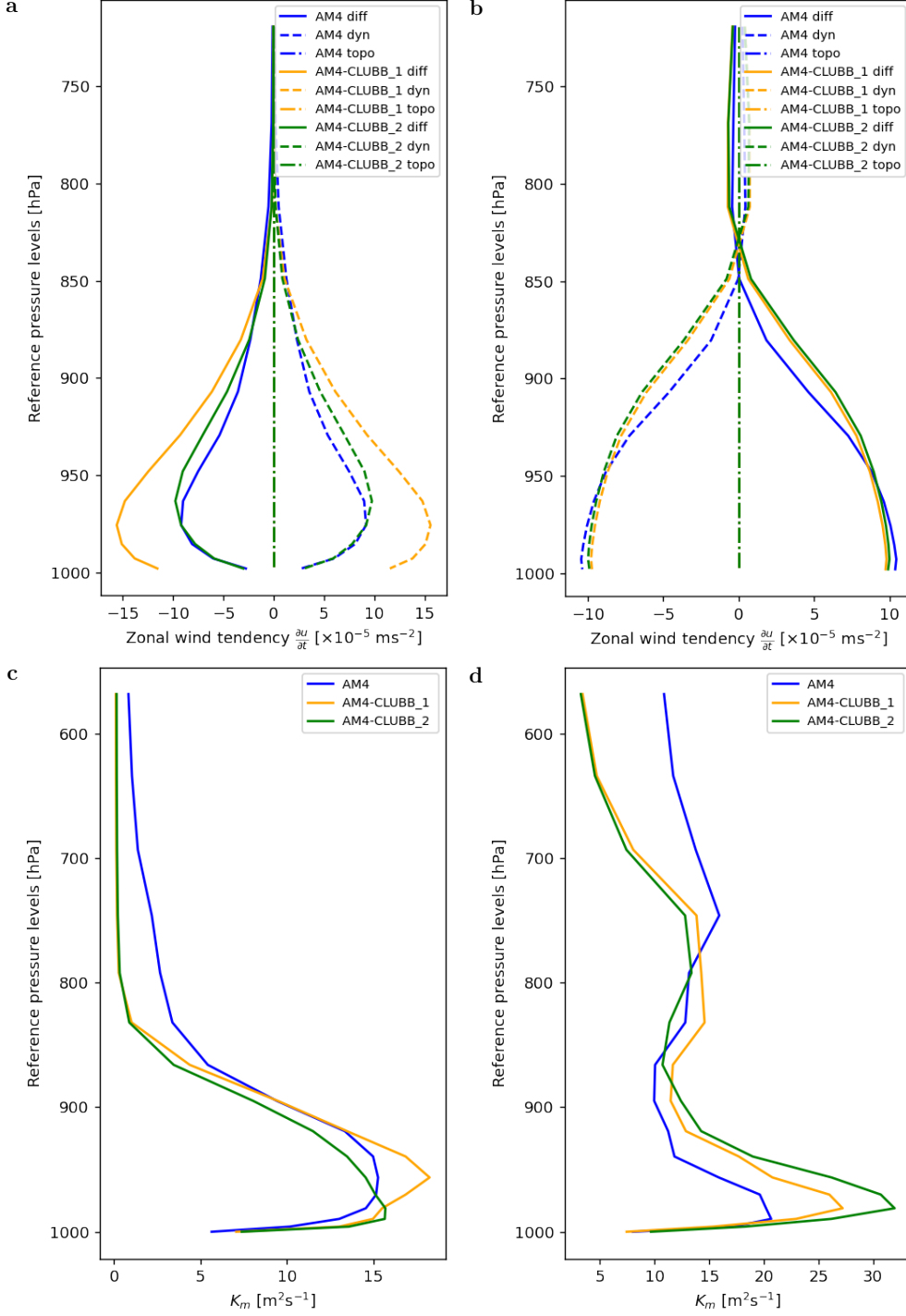


Figure 5. Zonal wind speed tendencies ($\frac{\partial u}{\partial t}$) and effective eddy momentum diffusivity coefficients (K_m) at specific locations in the Southern Ocean and the tropics. Panels (a) and (c) illustrate the vertical profiles of $\frac{\partial u}{\partial t}$ and K_m at a point in the Southern Ocean, specifically at 60°S latitude and 120°E longitude. Panels (b) and (d) display the corresponding profiles at a point in the tropics, located at 17°N latitude and 170°E longitude. The zonal wind speed tendency due to turbulent diffusion is labelled as “diff”, the zonal wind speed tendency due to dynamics is labelled as “dyn”, and the zonal wind speed tendency due to topography is labelled as “topo”. Because both points are over the ocean, the topography tendencies are zero for all configurations. The color scheme represents different simulations: blue for the control simulation AM4, orange for AM4-CLUBB_1, and green for AM4-CLUBB_2.

ing coupling strategy, as indicated by the unchanged potential temperature profile across AM4-CLUBB.1 and AM4-CLUBB.2. Conversely, the dynamic stability undergoes a notable increase in dynamic coupling AM4-CLUBB.2 compared to static coupling AM4-CLUBB.1, as can be inferred from the reduction in wind shear, with dynamic coupling AM4-CLUBB.2 aligning with the AM4 control simulation results. Such a shift implies less effective downward momentum diffusion and, consequently, reduced wind speeds. Although it may appear paradoxical that the enhanced diffusive damping can explain stronger winds, this may be better understood examining the different larger-scale dynamic forcing induced by the static and the dynamic coupling approaches, by comparing the maps of cross-section zonal wind speeds simulated by static coupling AM4-CLUBB.1 and dynamic coupling AM4-CLUBB.2 shown in Fig. 7. Indeed, the comparison of Fig. 7b and Fig. 7d shows that static coupling AM4-CLUBB.1 simulate a much more intense free-tropospheric zonal wind speed than dynamic coupling AM4-CLUBB.2 and control AM4. The most significant increase in wind speed occurs at the jet stream height (around 250 hPa), peaking at 5 m s^{-1} , resulting in a stronger lower-tropospheric wind shear in static coupling AM4-CLUBB.1 compared to AM4 (Fig. 7a-b). Instead, dynamic coupling reverses many of the changes introduced by static coupling, as illustrated in Fig. 7c-d. Consequently, even if static coupling AM4-CLUBB.1 and dynamic coupling AM4-CLUBB.2 would simulate the same effective eddy momentum diffusivity, the downward momentum transport remains stronger, under the static coupling approach. Therefore, the surface wind difference between AM4-CLUBB.1 and AM4-CLUBB.2 are largely influenced by the free-tropospheric wind difference. This implies that the decrease in PBL turbulent diffusion in AM4-CLUBB.2 relative to AM4-CLUBB.1 (discussed in Fig. 5,6), can be better attributed to diminished vertical wind shear in the lower-troposphere.

Turning our attention from the Southern Ocean to the tropics, here, the effect of changing the coupling strategy between surface momentum flux and CLUBB on $\frac{\partial u}{\partial t}$ and K_m vertical profiles is less pronounced than in the Southern Ocean, as previously highlighted by the analysis of the maps of near-surface wind speed changes (Fig. 2) and surface PBL characteristics (Fig. 3, Fig. 4). Figure 5b shows that the diffusion (labelled as “diff”) and dynamics (labelled as “dyn”) zonal wind speed tendencies for static coupling AM4-CLUBB.1 and dynamic coupling AM4-CLUBB.2 are nearly identical; additionally these tendencies are both only modestly reduced by 2 m s^{-2} compared to the control AM4. In Fig. 5d we see that this trend is mirrored in the profiles of the effective eddy diffusion coefficient K_m , showing that the effective eddy momentum diffusivity is also little responsive to changes in the coupling strategy. Analysis of the vertical profiles of zonal wind speed and potential temperature of both AM4-CLUBB.2 and AM4-CLUBB.1, shown in Fig. 6b,d, indicates a notably stronger agreement between them compared to the control simulation, AM4. Basing on zonal wind speed and potential temperature profiles, the PBLs of both AM4-CLUBB.2 and AM4-CLUBB.1 appear more unstable and thus more well mixed, with reduced wind shear near the surface. This may account for the larger K_m values of both AM4-CLUBB.1 and AM4-CLUBB.2 compared to AM4, resulting in the increased winds in the tropics found in Fig. 2. Thus, unlike in the Southern Ocean, it is the change from the Lock scheme in the control simulation (AM4) to the CLUBB scheme in the AM4-CLUBB.1 and AM4-CLUBB.2 simulations that primarily drives the variations found in the tropical PBL structure. Finally, the PBL differences being predominantly driven by the change in the PBL scheme rather than the coupling strategy with surface momentum flux could possibly be attributed to the two distinct dominant mechanisms of turbulent production across the tropics and the southern ocean as corroborated by the vertical profiles shown in Fig. 6: mechanical generation of turbulence in the Southern Ocean, and buoyancy (convection) in the tropics.

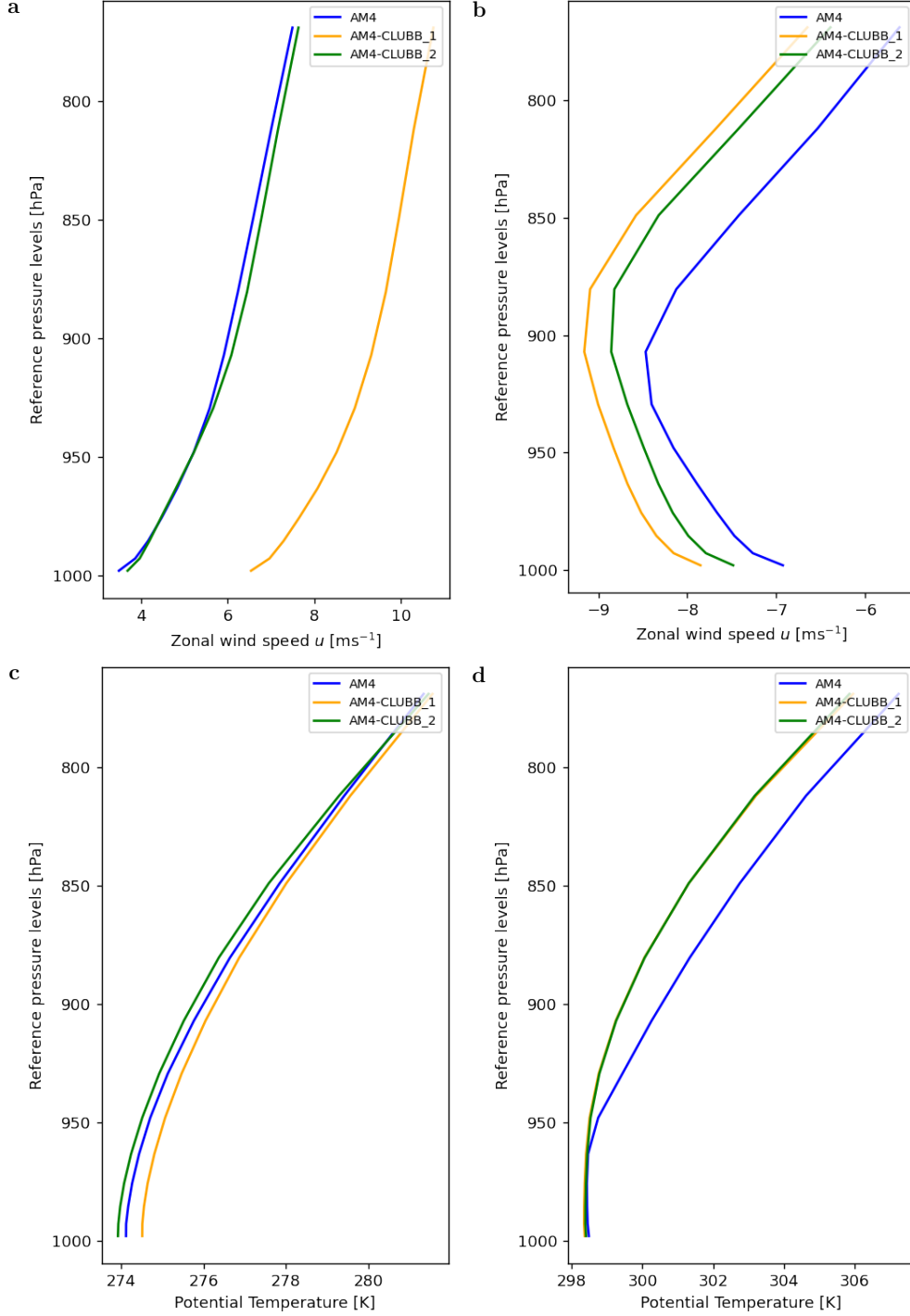


Figure 6. Vertical Profiles of Zonal Wind u and Potential Temperature θ at specific locations in the Southern Ocean and the Tropics. Panels (a) and (c) display the vertical profiles of zonal wind and potential temperature at a point in the Southern Ocean, specifically at 60°S latitude and 120°E longitude. Panels (b) and (d) present the corresponding profiles at a point in the tropics, located at 17°N latitude and 170°E longitude. The color coding represents different simulations: blue for the control simulation AM4, orange for AM4-CLUBB 1, and green for AM4-CLUBB 1 subcycle.

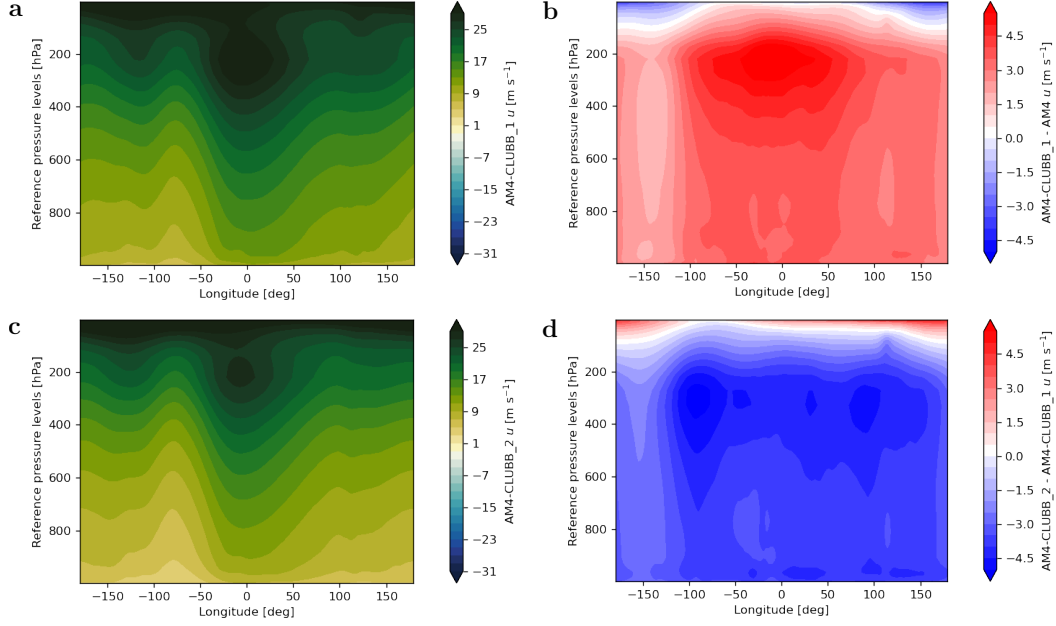


Figure 7. Vertical cross-section of zonal wind speed, u , at latitude 60°S for (a) AM4-CLUBB.1 and (c) AM4-CLUBB.2. Differences of vertical cross-section of zonal wind speed, u , between (b) AM4-CLUBB.1 and AM4 and (d) AM4-CLUBB.2 and AM4-CLUBB.1.

5 Evaluating the influence of coupling CLUBB with surface momentum flu on larger-scale circulation using the angle of wind turning metric

The examination of the vertical cross-section of zonal wind speed in the Southern Ocean revealed that modification in the coupling strategy between surface momentum flux and CLUBB can appreciably influence the overall atmospheric circulation. To attain a deeper understanding of such impacts, we evaluate the global spatial distribution of median wind turning angles across the three configurations used in this study: AM4, AM4-CLUBB.1, and AM4-CLUBB.2. The wind turning angle relates surface momentum flux, PBL turbulence, and cross-isobaric mass flux according to Eq. 5 (for more details, refer to Section 2.5). Our findings are visually presented in Fig. 8, which illustrates common patterns in the global distribution of wind-turning angles across all configurations. Notably, each model is characterized by clockwise (positive) turning in the Northern Hemisphere (NH) and counterclockwise (negative) turning in the Southern Hemisphere (SH). Furthermore, all configurations show a prevailing trend of increasing (in magnitude) wind turning angles with latitude (due to the increasing Coriolis parameter towards the poles), and more pronounced angles over land than over the ocean, corroborating previous studies (Lindvall & Svensson, 2019; Pyykkö & Svensson, 2023). However, a closer investigation of Fig. 8 reveals substantial differences among the control (AM4), static coupling (AM4-CLUBB.1), and dynamic coupling (AM4-CLUBB.2) model configurations. Specifically, the static coupling strategy between surface momentum flux and CLUBB employed in AM4-CLUBB.1 leads to large decreases (in magnitude) in the wind turning angle, particularly noticeable in the midlatitudes over the Southern Ocean, North Atlantic, and North Pacific Ocean, where reductions in median wind turning angles range between 10° and 15° . Land regions such as Siberia, North America, and Brazil experience even larger decreases in absolute value, with reductions of up to 20° . In contrast, transitioning to dynamic coupling strategy employed in AM4-CLUBB.2 substantially mitigates the underestimation observed with AM4-CLUBB.1. Specifically, AM4-CLUBB.2 exhibits a reduction in wind turning angles by two to three times in the mid-latitudes, aligning more closely with the AM4 control simulation's global

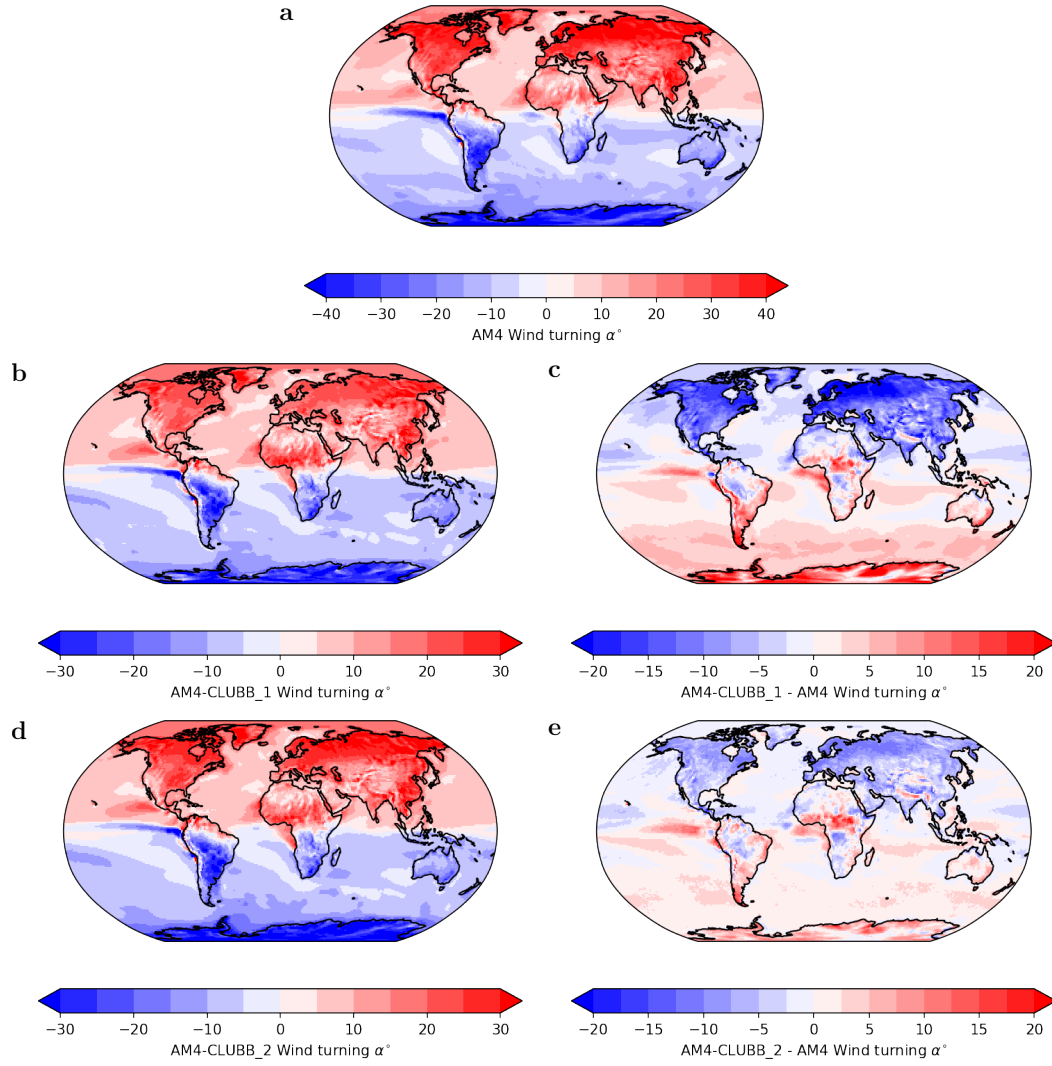


Figure 8. Maps of the median angle of wind turning from (a) AM4 (b) AM4-CLUBB.1 (d) AM4-CLUBB.2. Differences in the angle of wind turning between (b) AM4-CLUBB.1 and AM4 (e) AM4-CLUBB.2 and AM4.

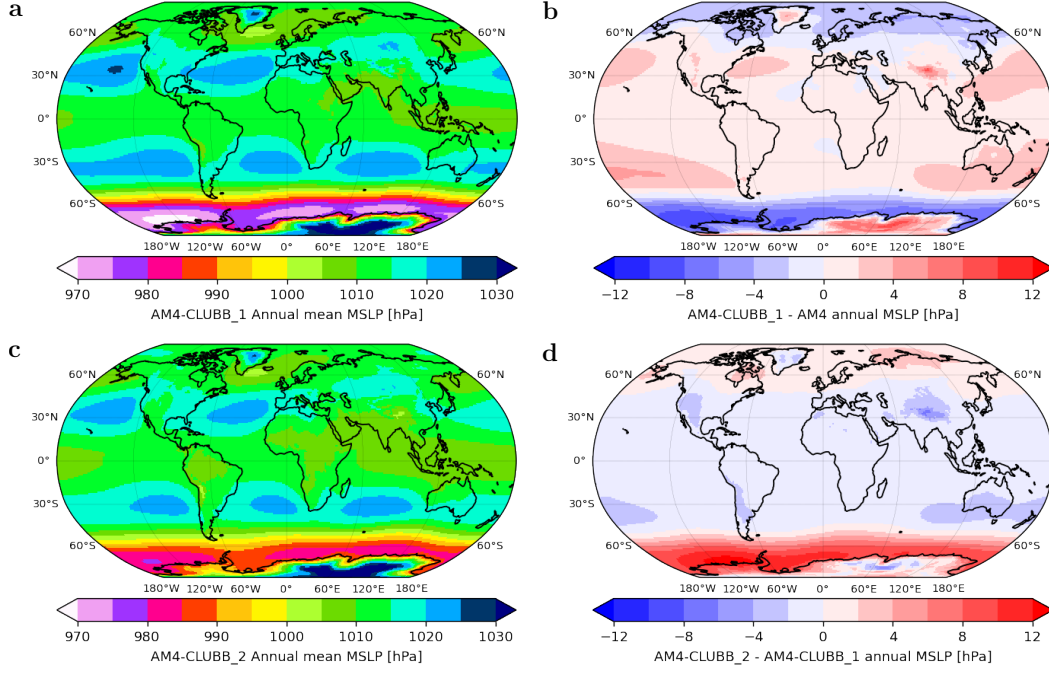


Figure 9. Mean sea level pressure (MSLP) simulated by (a) AM4-CLUBB_1, (c) AM4-CLUBB_2. MSLP difference between (b) AM4-CLUBB_1 and AM4 (d) AM4-CLUBB_2 and AM4-CLUBB_1.

distribution. For instance, over the Southern Ocean, AM4-CLUBB_2 reduces the underestimation of wind turning angles from approximately 15° to 5° . Nevertheless, in regions closer to the tropics and subtropics, dynamic coupling (AM4-CLUBB_2) wind turning angles are approximately equivalent to those observed with static coupling (AM4-CLUBB_1).

To better understand the relationship between changes in wind turning angle and impacts on the global circulation, we examine spatial maps of mean sea level pressure (MSLP) for both static (AM4-CLUBB_1) and dynamic coupling (AM4-CLUBB_2), comparing these to the baseline AM4 model and between each other, as depicted in Fig. 9. A careful examination of Fig. 9 reveals a strong correlation between the MSLP differences observed in static coupling (AM4-CLUBB_1) relative to control (AM4) with those found in wind turning angles. Specifically, in the Southern Ocean, AM4-CLUBB_1's MSLP reduction of up to 12 hPa, accompanied by an overestimation of up to 5 hPa in the Arctic, mirrors the adjustments in wind turning angles (refer to Fig. 9a-b). Meanwhile, in the tropics, where AM4-CLUBB_1's impact on wind turning angle is ambiguous, the MSLP variations are modest, around 2 hPa. Utilizing the dynamic coupling strategy between surface momentum flux and CLUBB (AM4-CLUBB_2) leads to distinct outcomes depending on the latitude of the regions under consideration (as shown in Fig. 9c-d). Notably, in mid-latitudes, an almost complete reversal of the MSLP changes introduced by static coupling (AM4-CLUBB_1) relative to control (AM4) occurs. For instance, in the Southern Ocean, dynamic coupling (AM4-CLUBB_2) amplifies the MSLP compared to static coupling (AM4-CLUBB_1) by up to 10 hPa, and by up to 4 hPa near the Arctic, effectively restoring the original MSLP distribution observed in control AM4. However, closer to the tropics, dynamic coupling slightly reduces MSLP, closely mirroring the MSLP values simulated by static coupling. These variations in MSLP are consistent with the changes in SH westerlies location and strength.

The correlation between changes in MSLP and changes in wind turning angles arising from the adoption of different coupling strategies, is further illuminated through Eq. 5, which delineates the relationship between wind turning angles and cross-isobaric mass flux.

According to Eq. 5, whose validity has been substantiated in the literature (Lindvall & Svensson, 2019; Pyykkö & Svensson, 2023), the reduced wind turning angles in the Southern Ocean, as found with AM4-CLUBB.1 compared to AM4, suggests an enhanced cross-isobaric mass flux. This increase in cross-isobaric mass flux, suggesting stronger convergence at the surface, indicates the formation of deeper low-pressure areas where the cross-isobaric mass flux is larger (and wind turning angles are smaller), especially in the midlatitudes which are dominated by the passage of low-pressure systems. This could explain the found reduction in both wind turning angle and MSLP within the static coupling (AM4-CLUBB.1) simulations, especially noted in the Southern Ocean between 50 and 70°S, and other midlatitudes ocean regions, near storm tracks. However, the relationship between reduced wind turning angles and MSLP is not uniform across all latitudes: for example between 30° and 50°S static coupling AM4-CLUBB.1 shows an increase in MSLP despite a decrease in wind turning angles, possibly attributed to the influence of surface friction on wind turning angles, as encapsulated in Eq. 5.

Further analysis into the dynamic coupling strategy of AM4-CLUBB.2 reveals that in regions above 50°S, a positive correlation exists between wind turning angles and MSLP, since increases in wind turning angles (relative to static coupling but still smaller than AM4) are aligned with MSLP increases, suggesting a reduced mass flux. Conversely, between 30 and 50°S, we observe MSLP increases alongside decreases in wind turning angles, likely due to heightened surface stress in dynamic coupling compared to static (between these latitudes only). Extending the comparison of MSLP and wind turning changes to the tropics, differences in wind turning angles between AM4-CLUBB.1 and AM4-CLUBB.2 are negligible, thereby implying that alteration in mass flux are insignificant, thus maintaining pressure patterns without appreciable deepening or weakening.

6 Conclusions

This study aimed to evaluate the impact of accurately coupling surface momentum flux with the CLUBB turbulence scheme on the simulation of near-surface wind speeds, associated momentum transport, and large-scale circulation patterns, utilizing the global climate atmospheric model version 4, AM4, developed by the GFDL. Towards this aim, three GFDL AM4 model configurations were used in this study, over 30 years from 1980 to 2010 to simulate present-day climate conditions: the control AM4 configuration (Zhao & et al, 2018), the AM4-CLUBB.1 configuration, using a static surface momentum flux coupling strategy which maintains a constant surface momentum flux throughout CLUBB's sub-stepping, and the AM4-CLUBB.2 configuration, using a dynamic coupling strategy, which updates the surface momentum flux at each CLUBB substep using the corresponding CLUBB-computed zonal and meridional wind speed tendencies.

In the examined simulations, we found that the static coupling approach (AM4-CLUBB.1 configuration), generates excessively strong global 10-m wind speeds, overestimating the corresponding values of both the ERA5 reanalysis dataset and the control AM4 simulations, particularly over the Southern Ocean. Conversely, the dynamic coupling approach between surface momentum flux and CLUBB (AM4-CLUBB.2) effectively corrects the pronounced bias in 10-meter wind speeds introduced by static coupling (AM4-CLUBB.1) in this region, but retains the same bias pattern of static coupling near the tropics. Comparison of dynamic and diffusion zonal wind speed tendencies and effective eddy diffusivity profiles at a selected location in the Southern Ocean where differences in 10-m wind speeds and associated PBL surface characteristics between static (AM4-CLUBB.1) and dynamic coupling (AM4-CLUBB.2) are most pronounced, notably demonstrates dynamic coupling (AM4-CLUBB.2) simulates the same turbulent momentum transport structure as the control AM4, while static coupling produces an excessively diffusive PBL. The investigation of zonal mean wind speeds differences between static and dynamic coupling revealed that much of the changes in PBL momentum diffusion can be attributed to larger-scale changes in the lower-tropospheric wind shear, which in turn control the near-surface wind speed dif-

ferences between static and dynamic coupling strategies. In tropical regions, changing from a static to a dynamic coupling strategy between surface momentum flux and CLUBB yields no appreciable changes in simulated 10-m wind speeds and the associated PBL momentum transport structure. Therefore, specific details of the PBL parametrization scheme play a more crucial role than the selected coupling strategy. This finding is consistent with earlier research indicating CLUBB potential to significantly modify the atmospheric structure over tropical regions, leading to increased precipitation, albeit with the associated excessive water vapor (Bogenschutz et al., 2013; Guo et al., 2015).

A plausible explanation for the distinct responses that we observed in the Southern Ocean and the tropics to the coupling strategies between CLUBB and surface momentum flux lies in the different mechanisms of turbulent momentum transport predominant in these regions. In the Southern Ocean, the mechanical generation of turbulence, often driven by the frequent passage of midlatitude cyclones, is likely to play a more significant role. Under this scenario, the reduction in surface momentum flux and near-surface wind speeds, as demonstrated by AM4-CLUBB_2 in comparison to AM4, would directly influence PBL vertical mixing by modifying wind shear dynamics. Conversely, in the tropics, buoyancy (or convection) is expected to dominate the turbulent kinetic energy budget, making this region more responsive to variations in surface heat and moisture fluxes than to changes in surface momentum fluxes.

The different atmospheric responses to the two coupling strategies between surface momentum flux and CLUBB were further investigated using the wind turning angle as a metric. The AM4 control simulation’s median wind turning angle, proven to outperform other CMIP6 models and the ERA-Interim reanalysis according to radiosonde observations (Pyykkö & Svensson, 2023), served as an optimal baseline for this analysis. Static coupling globally reduces the wind turning angle compared to control AM4, while dynamic coupling reverses these changes in the midlatitudes, in particular over the Southern Ocean, thus aligning the median wind turning angles more closely with those of the control simulation. This phenomenon may be attributed to dynamic coupling’s reduction in downward momentum flux compared to static coupling, promoting a more dynamically stable and stratified PBL atmosphere. Literature suggests that changes in static stability correlate with corresponding changes in wind turning angle (Lindvall & Svensson, 2019). Notably, using an equation that links the wind turning angle cosine to changes in cross-isobaric mass flux (Eq. 5), we qualitatively inferred that the dynamic coupling’s increased median wind turning angle over the Southern Ocean leads to reductions in the cross-isobaric mass flux. Consequently, this results in a shallower low-pressure pattern over that region compared to what is found by the static coupling approach. In contrast, in the tropics, dynamic coupling strategy does not produce appreciable changes in the median wind turning angle compared to the static coupling, with both approaches underestimating the AM4 wind turning angle values. This suggests that variations in wind turning angles within this region are more closely related to the choice of PBL parameterization scheme. Specifically, the employment of the CLUBB scheme for cloud and PBL turbulence parametrization appears to diminish the angle of wind turning, likely due to a decrease in PBL static stability as indicated by potential temperature profile analyses. The similar distributions of the angle of wind turning and associated PBL characteristics between static and dynamic coupling can then explain the similar MSLP patterns in the tropics, given that the cross-isobaric mass flux should also remain unchanged by the coupling strategy. Therefore the angle of wind turning turns out a useful qualitative metric to link changes in representation of surface momentum flux coupling strategies to changes the global circulation.

To summarize, the dynamic coupling strategy introduced in this study effectively brings CLUBB simulation of global near-surface wind speeds and associated momentum transport in line with the AM4 default configuration outcomes. Thus, it represents a robust framework to integrate more refined approaches into CLUBB to model turbulent momentum flux, such as directly prognosing turbulent momentum flux.

Data Availability statement

The ERA5 data by the European Centre for Medium-Range Weather Forecast (ECMWF) are available at <https://cds.climate.copernicus.eu/cdsapp#!/dataset/reanalysis-era5-single-levels>. The GFDL AM4 model is available at <https://github.com/NOAA-GFDL/AM4>.

Acknowledgments

This research was jointly funded as part of a Climate Process Team (CPT) under Grant AGS-1916689 from the National Science Foundation and Grant NA19OAR4310363 from the National Oceanic and Atmospheric Administration. We would also like to acknowledge Pu Lin (Princeton University/GFDL) for the help she gave on setting the AM4 model zonal wind speed tendency diagnostic.

References

- Best, M. J., Beljaars, A., Polcher, J., & Viterbo, P. (2004). A proposed structure for coupling tiled surfaces with the planetary boundary layer. *J Hydrometeor*, 5, 1271–1278.
- Bogenschutz, P., Gettelman, H., A. Morrison, Larson, V. E., Craig, C., & Schanen, D. P. (2013). Higher-order turbulence closure and its impact on climate simulations in the Community Atmosphere Model. *J Climate*, 26, 9655–9676.
- Bogenschutz, P., & Krueger, S. (2013). A simplified PDF parameterization of subgrid-scale clouds and turbulence for cloud-resolving models. *J Adv Model Earth Syst*, 5, 195–211.
- Bolot, M., Harris, L., Cheng, K., & et al. (2023). Kilometer-scale global warming simulations and active sensors reveal changes in tropical deep convection. *npj Clim Atmos Sci*, 6.
- Bryan, G., Worsnop, R., Lundquist, J., & Zhang, J. (2017). A simple method for simulating wind profiles in the boundary layer of tropical cyclones. *Bound.-Layer Meteor*, 162, 475–502.
- Bush, M., Allen, T., Bain, C., & et al. (2020). The first Met Office Unified Model–JULES Regional Atmosphere and Land configuration, RAL1. *Geosci Model Dev*, 13(4), 1999–2029. doi: 10.5194/gmd-13-1999-2020
- Catto, J., & et al. (2019). The future of midlatitude cyclones. *Curr Clim Change*, 5, 407–420.
- Cheng, A., & Xu, K.-M. (2008). Simulation of boundary-layer cumulus and stratocumulus clouds using a cloud-resolving model with low-and third-order turbulence closures. *Journal of the Meteorological Society of Japan. Ser. II*, 86A, 67–86.
- Danabasoglu, G., & et al. (2020). The Community Earth System Model version 2 (CESM2). *J Adv Model Earth Syst*, 12, 1–35.
- Donner, L., Seman, C., & Hemler, R. (2001). A cumulus parameterization including mass fluxes, convective vertical velocities, and mesoscale effects: Thermodynamic and hydrological aspects in a general circulation model. *J. Clim.*, 14, 3444–3463.
- Edwards, J., Beljaars, A., Holtslag, A., & et al. (2020). Representation of boundary-layer processes in numerical weather prediction and climate models. *Bound.-Layer Meteor*, 177, 511–539.
- Gang, C., Held, I., & Robinson, W. (2007). Sensitivity of the latitude of the surface westerlies to surface friction. *J Atmos Sci*, 64, 2899 - 2915.
- Golaz, J.-C., Larson, V., & Cotton, W. (2002a). A PDF-based model for boundary layer clouds. Part I: Method and model description. *J Atmos Sci*, 59, 3552–3571.
- Golaz, J.-C., Larson, V., & Cotton, W. (2002b). A PDF-based model for boundary layer clouds. Part II: Model results. *J Atmos Sci*, 59, 3552–3571.
- Guo, H., Golaz, J.-C., Donner, L. J., Ginoux, P., & Hemler, R. S. (2014). Multivariate probability density functions with dynamics in the GFDL atmospheric general circulation model: Global tests. *J Clim*, 27, 2087–2108.

- Guo, H., Golaz, J.-C., Donner, L. J., Wyman, B., Zhao, M., & Ginoux, P. (2015). CLUBB as a unified cloud parameterization: opportunities and challenges. *Geophys Res Lett*, *42*, 4540–4547.
- Haarsma, R. J., & et al. (2016). High resolution model intercomparison project (High-ResMIP v1.0) for CMIP6. *Geosci Model Dev*, *9*, 4185–4208.
- Han, J., Witek, M., Teixeira, J., Sun, R., Pan, H.-L., Fletcher, J., & Bretherton, C. (2016). Implementation in the NCEP GFS of a hybrid eddy-diffusivity mass-flux (EDMF) boundary layer parameterization with dissipative heating and modified stable boundary layer mixing. *Weather Forecast*, *31*, 341–352.
- Harris, L., Zhou, L., Kaltenbaugh, A., Clark, S. K., Cheng, K.-Y., & Bretherton, C. S. (2023). A global survey of rotating convective updrafts in the GFDL X-SHIELD 2021 global storm resolving model. *J Geophys Res Atmos*, *128*.
- Hersbach, H., Bell, B., Berrisford, P., & et al. (2020). The ERA5 global reanalysis. *Q J R Meteorol Soc*, *146*, 1999–2049.
- Khairoutdinov, M., & Randall, D. A. (2001). A cloud resolving model as a cloud parameterization in the NCAR community climate system model: Preliminary results. *Geophys Res Lett*, *28*, 3617–3620.
- Lappen, C.-L., & Randall, D. (2001). Toward a unified parameterization of the boundary layer and moist convection. Part I: a new type of mass-flux model. *J Atmos Sci*, *58*, 2021–2036.
- Lappen, C.-L., Randall, D., & Yamaguchi, T. (2010). A higher-order closure model with an explicit PBL top. *J Atmos Sci*, *67*, 834–850.
- Larson, V., Domke, S., & Griffin, B. M. (2019). Momentum transport in shallow cumulus clouds and its parameterization by higher-order closure. *J Adv Model Earth Syst*, *11*, 3419–3442.
- Larson, V., & Golaz, J. (2005). Using probability density functions to derive consistent closure relationships among higher-order moments. *Mon Weather Rev*, *133*, 1023 – 1042.
- Larson, V., Schanen, D., Wang, M., Ovchinnikov, M., & Ghan, S. (2012). PDF parameterization of boundary layer clouds in models with horizontal grid spacings from 2 to 16 km. *Mon Weather Rev*, *140*, 285–306.
- Lindvall, J., & Svensson, G. (2019). Wind turning in the atmospheric boundary layer over land. *Q J R Meteorol Soc*, *145*, 3074–3088.
- Lock, A., Brown, A., Bush, M., Martin, G., & Smith, R. (2000). A new boundary layer mixing scheme. Part I: scheme description and single-column model tests. *Mon Weather Rev*, *128*, 3187–3199.
- Mbengue, C., & Woollings, T. (2019). The eddy-driven jet and storm-track responses to boundary layer drag: Insights from an idealized dry GCM study. *J Atmos Sci*, *76*, 1055 - 1076.
- Molina, M. O., Gutiérrez, C., & Sánchez, E. (2021). Comparison of ERA5 surface wind speed climatologies over Europe with observations from the HadISD dataset. *Q J R Meteorol Soc*, *144*, 943—969.
- Nardi, K. M., Zarzycki, V. E., C. M. Larson, & Bryan, G. H. (2022). Assessing the sensitivity of the tropical cyclone boundary layer to the parameterization of momentum flux in the Community Earth System Model. *Mon Weather Rev*, *150*, 883–906.
- Palmer, T. (2014). Climate forecasting: Build high-resolution global climate models. *Nature*, *515*, 338–339.
- Polcher, J., & et al. (1998). A proposal for a general interface between land-surface schemes and general circulation models. *Global Planet Change*, *19*, 263–278.
- Pyykkö, J., & Svensson, G. (2023). Wind turning in the planetary boundary layer in CMIP6 models. *J. Climate*, *23*, 5729–5742.
- Randall, D., Khairoutdinov, M., Arakawa, A., & Grabowski, W. (2003). Breaking the cloud parameterization deadlock. *Bull Am Meteorol Soc*, *84*, 1547–1564.
- Randall, D., Shao, Q., & Moeng, C. (1992). A second-order bulk boundary-layer model. *J Atmos Sci*, *49*, 1903–1923.

- 790 Rotstayn, L. (1997). A physically based scheme for the treatment of stratiform clouds and
791 precipitation in large-scale models. I: Description and evaluation of the microphysical
792 processes,. *Q J R Meteorol Soc*, *123*, 1227-1282.
- 793 Schär, C., Fuhrer, O., Arteaga, A., & et al. (2020). Kilometer-scale climate models:
794 prospects and challenges. *Bulletin of the American Meteorological Society*, *101*, 567-
795 587.
- 796 Siebesma, A., Soares, P., & Teixeira, J. (2007). A combined eddy-diffusivity mass-flux
797 approach for the convective boundary layer. *J Atmos Sci*, *64*, 1230-1248.
- 798 Slingo, J., Bates, P., Bauer, P., & et al. (2022). Ambitious partnership needed for reliable
799 climate prediction. *Nat Clim Chang*, *12*, 499-503.
- 800 Stevens, B., Satoh, M., & Auger, L. e. (2019). Dyamond: the dynamics of the atmospheric
801 general circulation modeled on non-hydrostatic domains. *Prog Earth Planet Sci*, *6*.
- 802 Svensson, G., & Holtslag, A. (2009). Analysis of model results for the turning of the wind
803 and related momentum fluxes in the stable boundary layer. *Bound.-Layer Meteor*,
804 *132*, 261-277.
- 805 Tan, Z., Kaul, C. M., Pressel, K. G., Cohen, Y., Schneider, T., & Teixeira, J. (2018). An
806 extended eddy-diffusivity mass-flux scheme for unified representation of subgrid-scale
807 turbulence and convection. *J Adv Model Earth Syst*, *10*, 770–800.
- 808 Tiedtke, M. (1993). Representation of clouds in large-scale model. *Mon Weather Rev*, *121*,
809 3040-3061.
- 810 Troen, I., & Mahrt, L. (1986). A simple model of the atmospheric boundary layer; sensitivity
811 to surface evaporation. *Bound.-Layer Meteor*, *37*, 129-148.
- 812 Wang, M., Larson, V., Ghan, S., Ovchinnikov, M., Schanen, D., & Xiao, H. e. (2015).
813 A multiscale modeling framework model (superparameterized CAM5) with a higher-
814 order turbulence closure: Model description and low-cloud simulations. *J Adv Model
815 Earth Syst*, *7*, 484-509.
- 816 Wyant, M., Bretherton, C., Rand, H., & Stevens, D. (1997). Numerical simulations and a
817 conceptual model of the stratocumulus to trade cumulus transition. *J Atmos Sci*, *54*,
818 168-192.
- 819 Zhao, M., & et al. (2018). The GFDL global atmosphere and land model AM4.0/LM4.0: 2.
820 Model description, sensitivity studies, and tuning strategies. *J Adv Model Earth Syst*,
821 *10*, 735–769.